Nanoincorporation of iron oxides into carrageenan gels and magnetometric and morphological characterizations of the composite products

Kazuyuki Oya, Takahiro Tsuru, Yoshikuni Teramoto, and Yoshiyuki Nishio*

Division of Forest and Biomaterials Science, Graduate School of Agriculture, Kyoto University, Sakyo-ku, Kyoto 606-8502, Japan

*To whom correspondence should be addressed. Phone: +81-75-753-6250, Fax: +81-75-753-6300, E-mail: ynishio@kais.kyoto-u.ac.jp.

RUNNING HEAD :

Magnetic iron oxide-incorporated carrageenan composites

Keywords: Carrageenan; *in situ* synthesis; iron oxide; magnetic nanocomposites; superparamagnetism

ABSTRACT: Carrageenan-based magnetic composites were prepared via *in situ* synthesis of iron oxides in a gelatinous network of the polysaccharide. The repeatable synthesis process involved three steps: immersion into ferrous salt ($FeCl_2$) solution, alkali treatment in sodium hydroxide solution, and oxidation with hydrogen peroxide, successively performed on *ι*- or *κ*-carrageenan hydrogels as the starting material. FE-SEM observations, X-ray diffractometry, and SQUID magnetometry were carried out for the freeze-dried composites. Feroxyhite, and magnetite and/or maghemite particles were produced after one cycle and multicycles of the *in situ* process, respectively, in a size less than several tens of nanometers and distributed in the inside as well as on the surface of numerous fibrillar entities constituting the carrageenan matrix used. Almost all the composite products explored displayed a superparamagnetic (SPM) property at 298 K; the estimated saturation magnetization (M_s) heightened with increasing concentration of $FeCl_2$ in the gel immersion step and with repetition of the standardized process of iron oxide synthesis. By repeating the synthesis cycle 3–4 times, a composite of practically high M_s reaching ~25 emu (g sample)$^{-1}$ was easily obtainable without impairing the SPM character. Insight was provided into the evolution mechanism in oxidation state and dimensional distribution of the cyclically loaded iron oxide nanoparticles, through comparison with another composite series obtained by a coprecipitation method with a 1:2 mixture of ferrous/ferric salts.

INTRODUCTION

Polymer/inorganic nanocomposites are usually defined as polymer materials containing a smaller amount of inorganic particles structured at an average scale (in diameter or thickness) of less than several tens of nanometers. They are expected to be indispensable in future engineering technologies including biomaterial designing. As a functional development of carbohydrate polymers towards advanced materials, the designing of magnetic nanocomposites based on cellulose[1–8] and related polysaccharides[6,9–15] has attracted much attention since the early 1990s, because of the potential applications including information transfer or storage media, fabrics for electromagnetic shielding, new filtration and separation systems, magnetic drug-delivery systems, and so on. *In situ* synthesis of iron oxide particles in fibrillar suspensions or gels of polysaccharides was a useful chemical technique for the nanocompositions. As initially proposed by Ziolo et al.[16] and Marchessault et al.,[1] a typical route for preparing the composite samples consists of the following steps: (1) ferrous ion-absorption of the original polymer materials following their swelling or gelation in a ferrous salt solution (e.g. aqueous $FeCl_2$ or $FeSO_4$); (2) *in situ* precipitation of ferrous hydroxide by treatment of the swollen polymers with aqueous hydroxide of alkali or alkali-earth metal; (3) oxidation of the ferrous hydroxide with an oxidizing agent (e.g. H_2O_2) or O_2-bubbling. It is worthy of special remark that the composites obtained by such an *in situ* synthesis method can exhibit superparamagnetism (SPM) at ambient temperature; that is, there appears no remanent magnetization (M_r) and coercive force (H_c) in measurements of magnetization (M) vs applied magnetic field (H), in contrast to the common ferro(i)magnetism (FM) showing a definite hysteresis loop. That unique magnetic character can be observed when the magnetic particles are dispersed in the matrix on a scale of less than a few tens of nanometers, the product being qualified exactly as a nanocomposite.

The process standardized above should be made best expedient in the reaction conditions

and chemicals adopted, according to the target system of composition or the polymer subject employed. In the authors' laboratory, previously, an interpenetrating network (IPN) type of alginate/poly(vinyl alcohol) gels containing iron oxide nanoparticles was constructed through adequate modification of the *in situ* ferrite synthesis technique; the gelation and alkali treatment were carried out with the aid of a metallic borate.[14] The IPN gels were designed to acquire a variable viscoelastic property in addition to the SPM perceptibility to an external magnetic stimulus. Recently, we also succeeded in fabrication of a see-through woody magnetic sheet showing SPM, via a sequence of procedures including chemical modification of wood flour (WF), nanoincorporation of iron oxides into the WF matrix, and hot-molding of the WF/iron oxide composite.[7]

The standard process of (1)–(3) may be repeated several times for the purpose of elevating the iron content and enhancing the oxidation or alteration of the iron compounds precipitated;[2,3] ordinarily, this repetition will heighten the value of saturation magnetization (M_s) of the resulting composite. Then a target is again an SPM character, but with quite a high M_s (e.g. >25 emu (g sample)$^{-1}$).[2] Thereby, while the material is sharply and largely magnetized by a modest H, it never retains the magnetization if the external field is removed. This would be particularly desirable for the use as a core material of actuators responsive to magnetic stimuli.

A polymer matrix used in the present work is carrageenan, which is a sulfated galactan derived from red seaweeds.[17] Conventionally available carrageenans are of ι, κ, and λ types; ι- and κ-carrageenan polymers (see the structural formula in Figure 1) possess a hydrogel-forming ability, whereas λ-carrageenan scarcely does.[17–19] The gelation and solution behavior of the former two carrageenans in water is thermo-reversible, and the gel networks formed at lower temperatures (usually <70 ºC) are more stabilized in the presence of alkaline or alkali-earth metallic cations.[18,19] In those gels, the cations seem to promote a side-by-side association of carrageenan chains partly assuming a double-helical fashion.[19]

As was suggested in a previous paper,[11] multivalent cations of the iron-group elements (Fe, Co, and Ni) could also act as an effective stabilizer of carrageenan gels.

<<**Figure 1**>>

In the present paper, we would like to demonstrate that superparamagnetic carrageenan composites loaded with iron oxide nanoparticles can be easily prepared so as to exhibit an M_s value as high as 25 emu (g sample)$^{-1}$. Insight is provided into an effect of the repetition of that synthesis cycle on the evolution in oxidation state of the magnetic particles, as well as into some differences in magnetometric profiles between the two cases using either *ι*- or *κ*-carrageenan as the matrix polymer. Further, a comparative characterization is made for carrageenan-based composites prepared by a stoichiometric coprecipitation method[20] with a 1:2 mixture of ferrous/ferric salts; this technique has also been applied to the iron oxide nanocompositions with diverse polysaccharides.[4,5,8,11–13,15]

EXPERIMENTAL

Original Materials

The polymer samples used were commercially available *ι*-carrageenan (Copenhagen Pectin Ltd., GENUGEL CJ, lot no. 016822; $M_w = 8.52\times10^5$, $M_w/M_n = 2.49$, and S = 7.65 wt%) and *κ*-carrageenan (Copenhagen Pectin Ltd., GENUGEL WR-78-J, lot no. 035400; $M_w = 8.28\times10^5$, $M_w/M_n = 2.21$, and S = 5.97 wt%). The data of sulfur (S) content were obtained through elemental analysis, and the values of weight-average molecular mass (M_w) and polydispersity (M_w/M_n) were determined by GPC chromatography (mobile phase, 75 mM sodium nitrate aqueous solution at 40 ºC) in comparison with poly(ethylene oxide) standards.

Ferrous chloride tetrahydrate ($FeCl_2\cdot4H_2O$) and H_2O_2 aqueous solution were obtained from Wako Pure Chemical Industries, Ltd., and all the other chemicals and solvents used were guaranteed reagent-grades. They were employed without further purification.

Preparation of Iron Oxide-Containing Carrageenan Composites

The following procedures for *in situ* synthesis of iron oxides in the gelatinous carrageenan matrix were carried out in an atmosphere of nitrogen, except for an oxidizing step. The distilled water and ethanol used were degassed with N_2-bubbling. A volume ratio of ethanol/water used as a mixed solvent was always 1:1.

The original powder of carrageenan of ι or κ type was dissolved in distilled water at ~95 ºC. A portion of the aqueous solution (polymer conc., 3–8 wt%) was put into a syringe and cooled. Subsequently, the solution, already gelatinous but transparent and colorless, was injected in a long cylindrical form (ϕ = ~2.5 mm) into an excess amount of ethanol/water (20 ºC) containing $FeCl_2$ at a concentration of 0.01–0.50 M. After immersion in the salt solution for 2 h, the ferrous carrageenan gel, imparting a slightly yellowish hue, was lightly washed with ethanol/water and then steeped in 1.0 M NaOH/ethanol/water (pH ≈ 13) for 2 h. The alkaline solution bath (~150 mL) was heated to ~65 ºC and 2 wt% H_2O_2 solution (~15 mL) was added therein dropwise over a period of 1 h. The oxidized gel, colored dark reddish brown, was washed with ethanol/water and lyophilized (especially for magnetometry and FE-SEM observations) or vacuum dried.

Selected gel samples oxidized once in the above-mentioned way were further oxidized in additional cycles involving the ferrous ion-absorption, alkali treatment, and oxidation with hydrogen peroxide. In what follows, a code "*x*% ι-*y*-*n*" denotes a product sample obtained after *n* cycles of the reaction scheme by using a starting *x* wt% ι-carragenan aqueous solution to be gelled in *y* M ferrous chloride/ethanol/water. For κ-carrageenan-based products, a similar code "*x*% κ-*y*-*n*" is defined.

A coprecipitation method with a stoichiometric mixture of Fe^{2+}/Fe^{3+} = 1:2 (mol/mol) was applied to obtain κ-carrageenan-based composites for comparison. An aqueous solution of the polymer was prepared at 5 wt% in the same way as that described above. A portion of the cooled solution (gelatinous) was immersed in a 1:2 ferrous/ferric chloride solution in

ethanol/water (20 ºC) over a time period of 2 h. The salt solution was prepared at 0.10 M in respect of the total iron ions, by dissolving $FeCl_2 \cdot 4H_2O$ and $FeCl_3 \cdot 6H_2O$ in the solvent to yield the adequate Fe^{2+}/Fe^{3+} proportion specified above. Subsequently, the κ-carrageenan gel was, in turn, immersed in 1.0 M NaOH/ethanol/water at ~68 ºC without agitation for 24 h, and then thoroughly washed with ethanol/water under an ordinary atmospheric condition. Selected samples of the dark-brown composite gels thus prepared were subjected to additional cycles of the same route. A solid product freeze-dried after *n* cycles is designated as "5% κ-0.10(cop)-*n*" hereinafter.

Measurements

The iron content in the respective composites described above was determined by a redox titration method. Iron ions were extracted from a weighed fragment of each dried composite with a warmed HCl solution, then reduced to Fe^{2+} with the aid of tin(II) chloride. The ferrous ionic solution was titrated with potassium dichromate by using diphenylamine-4-sulfate as an indicator.

Fourier transform infrared (FT-IR) spectra of carrageenan samples were obtained at each stage of the *in situ* synthesis of iron oxides, by using a Shimadzu FTIR-8000 spectrometer purged with N_2 gas in advance. An ordinary KBr pellet method was adopted for the measurements. Especially after the step of ferrous ion-absorption, and after the alkali treatment step as well, the samples were ground and mixed with KBr under a nitrogen atmosphere.

Wide-angle X-ray diffraction (WAXD) measurements were carried out with a Rigaku RINT2200V diffractometer at room temperature (20 ºC) in a reflection mode. Nickel-filtered CuKα radiation was used at 40 kV and 30 mA. Diffraction intensity profiles mainly in a range of 2θ = 25–65º were collected to identify the iron oxide particles synthesized in the carrageenan matrix.

Fracture-surface morphologies of carrageenan/iron oxide composites were observed by using a field emission scanning electron microscope (FE-SEM), Hitachi S-4500; the fractured samples were sputter-coated with platinum before the observation. Transmission electron microscopy (TEM) with JEOL JEM-1220 was also conducted to inspect the dimension of the iron oxide particles present in the composites. The sample for this observation was prepared on a microscope grid from an aqueous micro-suspension of iron oxide residues. The suspension was made through dissolution of carrageenan constituting the composite concerned into distilled water.

Magnetometry measurements were carried out on 5–7 mg samples (freeze-dried) with a superconducting quantum interference device (SQUID), MPMS-5 of Quantum Design Inc. The magnetic field (H) applied was usually varied as $0 \rightarrow 5$ T $\rightarrow -0.1$ T $\rightarrow 0$ at a constant temperature. For a given sample, data of the magnetization (M) vs H were collected at 298, 200, and 100 K. With regard to a few selected series of carrageenan composites, temperature dependence of magnetization was examined in the so-called zero-field-cooled (ZFC) and field-cooled (FC) conditions. First, for the ZFC magnetization, the sample was cooled to 5 K with the magnetic field set at zero. After stabilization at 5 K for 20 min, a magnetic field of 0.01 T was applied to the regulated sample, and the magnetization M was evaluated. The measurement was done consecutively while the temperature was increased from 5 to 300 K at 20 K increments. Following this ZFC experiment, the same sample was then cooled from 300 to 5 K under a constant filed of 0.01 T, and, concomitantly, the FC magnetization data were accumulated every 20 K.

RESULTS AND DISCUSSION

Magnetization (M) vs Applied Field (H) Behavior

All the composite products prepared via the three chemical steps (see above) were responsive to a conventional bar magnet, evidently attracted by this; but they were all visually

inert to steel materials at ambient temperature.

Figure 2a illustrates magnetization behavior of a series of 5% *ι*-0.10-*n* at 298 K as a function of applied magnetic field. Any of the samples of n = 1–3 exhibits a characteristic M vs H profile in which a steep magnetization occurs and there appears no remanent magnetization (see an inset of the figure), i.e., the magnetism can be regarded as SPM. For estimation of the saturation magnetization M_s, the respective data in a range of 0–5 T were regressed in terms of the following classical Langevin function,[21]

$$M = M_s [\coth(\alpha) - \alpha^{-1}] \qquad (1)$$

with $\alpha = \mu H/k_B T$, where μ is a magnetic moment per particle, k_B is the Boltzman constant, and T denotes absolute temperature. Values of M_s = 2.9 (n = 1), 14.3 (n = 2), and 21.9 (n = 3) in emu (g sample)$^{-1}$ were estimated, demonstrating that the cyclic repetition of the *in situ* synthesis resulted in a marked elevation in M_s.

<<**Figure 2 (a) & (b)**>>

In Figure 2b, an M vs H data for the sample 5% *ι*-0.10-3 at 100 K is compared with that obtained at 298 K. As shown on an enlarged scale in an inset of the figure, the sample imparted a hysteresis in the range of −0.05–0.05 T at 100 K; that is, the magnetism is judged to be FM at this low temperature, differing from the situation at 298 K.

Magnetic properties of iron oxide-containing carrageenan composites prepared under different conditions are summarized in Table 1. In this tabulation, three or four samples on family terms are grouped in a series, to be able to roughly recognize the diversity of data that arises from altering one of the preparation conditions.

<<**Table 1**>>

As can be seen from the comparison between the two series 5% *ι*-*y*-1 and 5% *κ*-*y*-1, the dependence of the Fe amount loaded into a polymer matrix on the ferrous ion concentration (y) in gel immersion is stronger in the *κ*-carrageenan series. A similar observation refers to the concentration dependence of M_s (per gram sample) at 298 K, when compared between the

same two series. To show this more explicitly, plots of M_s vs Fe^{2+} concentration are constructed in Figure 3a, where data are compiled for all the ι- and κ-carrageenan composites of $n = 1$ explored. Irrespective of the starting polymer concentration (x), the ι-carrageenan series showed a relatively gradual slope in the plot, while the κ type-based series made a steeper one. As is well known,[17–19] ι-carrageenan gels significantly strengthen in the presence of divalent cations such as Ca^{2+}, differing from the modest hardening of κ-carrageenan gels; contrastively, however, many of the monovalent cations promote the gelation of κ-carrageenan rather than ι-carrageenan. Ferrous cation would work on ι-carrageenan in the same way as Ca^{2+} to tighten the gel structure, which was actually discerned by manipulation. As a result, comparatively smaller particles of iron oxide could be produced in the tighter network system of ferrous ι-carrageenan, but with a wide distribution over the whole polymer matrix. As the case stands, we find a tendency that the ι-carrageenan composite series retains the SPM character to lower temperatures, relative to the κ-carrageenan series (see Table 1).

<<**Figure 3 (a), (b), & (c)**>>

In Figure 3b, the dependence of M_s at 298 K on the cycle number n of the *in situ* synthesis of iron oxides is shown for ι- and κ-carrageenan composite series, which were prepared at a starting polymer concentration of 3 or 5 wt% and with a 0.10 M ferrous salt solution in the gel immersion step. It is evident that, irrespective of the type of carrageenan, M_s increases drastically with the cycle number. The value exceeds 20 emu $(\text{g sample})^{-1}$ in the treatment of $n = 3$, and, regarding ι-carrageenan-based examples of $n = 4$ and 5, it is well over 25 and 30 emu $(\text{g sample})^{-1}$, respectively. The magnetism at 298 K of the sample encoded as 5% ι-0.10-5 is marked FM in Table 1, but the hysteresis loop observed in a range of $H = -0.01$–0.01 T was quite narrow ($H_c < 10^{-3}$ T, $M_r < 1$ emu $(\text{g sample})^{-1}$). Thus the repetition of the reaction cycle is found to be much more effective in elevating M_s at a high rate of increment, rather than conditionings of the starting polymer concentration and even the

ferrous ion concentration.

Saturation magnetization data were also assembled in a specific value (M_s(Fe)) that was normalized with Fe content for each composite sample. As seen in Table 1, most of the composites of n = 1 gave a specific M_s(Fe) of 34 ± 4 emu (g Fe)$^{-1}$, without showing any dependence on the polymer and Fe^{2+} concentrations in the initial gel treatment. In Figure 3c, plots of M_s(Fe) vs the cycle number are constructed for the same series of samples as those used in Figure 3b. In a major trend, as the reaction cycle is repeated, the specific value increases, but the rate of the increment becomes gradual so as to make a convergence of M_s(Fe). This result suggests that the iron oxides incorporated into any of the composites of n = 1 are mainly of lesser magnetic (e.g. ferric oxyhydroxide), and the repetition of $n \geq 2$ raises a proportion of more familiar magnetic particles such as ferric oxide (e.g. γ-Fe_2O_3) and ferrous ferric oxides (e.g. Fe_3O_4).

Morphology of Iron Oxide-Containing Carrageenan Composites

Figure 4 shows FT-IR spectra for ι-carrageenan samples obtained at each stage of the *in situ* synthesis of iron oxides, the final product corresponding to 5% ι-0.10-1. In this figure, the spectrum (i) was measured for a purified ι-carrageenan powder prepared by reprecipitation in ethanol from aqueous solution. An important absorption band to deserve attention is the ester sulfate signal appearing as dual peaks in a wavenumber range of 1200–1300 cm^{-1}. With regard to the sample of ferrous ion-intercalated ι-carrageenan (see (ii) in Fig. 4), the S-O asymmetric stretching peak shifted to 1210 cm^{-1} from the original position of 1230 cm^{-1}, accompanied by broadening of the sulfate signal as a whole. This observation implies an electrostatic interaction between the sulfate group and Fe^{2+}, which also supports the stabilization of the gel structure with the divalent cation. By the following alkali treatment, the sulfate band was restored to its original figure (see (iii) in Fig. 4), indicating that the intercalated Fe^{2+} ions were liberated from the sulfate groups and consumed

to produce ferrous hydroxide in the polymer network. Even via the subsequent step of oxidation, the absorption band was no longer changed (see (iv) in Fig. 4). An additional measurement was made for a sample 5% *ι*-0.10-3 subjected to three cycles of the sequential reactions, but the spectrum was essentially the same as (iv).

<<**Figure 4**>>

IR investigation was also performed on a *κ*-carrageenan-based series and a similar result to the above was acquired, as far as the observations on the ester sulfate band in the 1200–1300 cm^{-1} region were concerned; however, the spectral feature of *κ*-carrageenan was different in places from that of *ι*-carrageenan in the side of lower wavenumbers (600–1100 cm^{-1}). In the present IR measurements, it was difficult to find a clear difference in gel structure or interaction strength with Fe^{2+} between the two types of carrageenan.

Fracture-surface morphologies of carrageenan/iron oxide composites were examined by FE-SEM. Figure 5 shows micrographs obtained for lyophilized *ι*- and *κ*-carrageenan gels containing ion oxides (photos **c**, **e**, and **g**), in comparison with their respective reference samples of naught Fe content (photos **a**, **b**, **d**, and **f**). The reference samples were prepared without immersing the gels into ferrous chloride solution (expediently the parameter $y = 0$) in the cycle of *in situ* synthesis; however, an exceptional sample encoded as 5% *ι*-0.10(Ca)-1 underwent the gel immersion step, but with $CaCl_2$ instead of $FeCl_2$ at 0.10 M. As demonstrated by the micrographic data **d** and **f**, the blank samples of *κ*-carrageenan gels are well endowed with fibrous and porous structures in the interior; we can see numerous fibrillar entities of a few tens of nanometers in width percolate through the matrix space, with lateral coalescences and thick junctions from place to place. The percolation morphology of fibrils was also prevalent in iron oxide-incorporated *κ*-carrageenan gels, which was confirmed by FE-SEM observations at relatively low magnifications. However, the fibrillar entities were full of humps after one cycle treatment of the *in situ* reactions, and after three repetitions of the cycle, the apparent aspect ratio of fibrils was considerably lowered; these are evidenced by

the enlarged micrographs **e** (for 3% κ-0.10-1) and **g** (for 3% κ-0.10-3) in Figure 5. As represented schematically in the insets put into the photos **e** and **g**, it is supposed that the inorganic nanoparticles were dispersed in the inside as well as on the surface area of fibrillar entities constituting the polymer matrix, possibly the fibrils being partly sectioned.

<<**Figure 5 (a)–(g)**>>

With regard to the ι-carrageenan series, the blank samples prepared without supply of ferrous ions, but exposed to sodium monovalent cations in the alkali treatment, formed a weak gel; the interior was generally poor in ramified fine fibrils and made up of more thickset entities 100–150 nm in width, as exemplified by photo **a** in Figure 5 taken for 5% ι-0-1. In contrast to this, another reference sample that underwent the gel immersion with divalent calcium cations, such as 5% ι-0.10(Ca)-1, showed a well-developed fibrous structure (see photo **b** in Fig. 5). Probably, a similar fibrous architecture would develop more or less in the ι-carrageenan gels treated with ferrous ions, and iron oxide particles should be produced inward and on the fibrils in the subsequent oxidation step, eventually, in the same manner as that observed for the κ-carrageenan-based composite gels. In Figure 5, this is proved by a morphology illustrated for 5% ι-0.10-1 (photo **c**), although the exemplified fibrillar structure is somewhat rugged compared with that seen in the data **e** for 3% κ-0.10-1.

Figure 6 illustrates WAXD intensity profiles for 5% ι-0.10-n (n = 1–3), and 2θ values of the observed diffraction peaks are listed in Table 2 and they are compared with the corresponding data of JCPDS (Joint Committee on Powder Diffraction Standards) for Fe_3O_4 (JCPDS card no. 19-629), γ-Fe_2O_3 (JCPDS card no. 39-1346), and δ-FeOOH (JCPDS card no. 13-87). Judging from the comparison, the iron oxides incorporated into the composite of n = 1 are mainly feroxyhite (δ-FeOOH) showing a weaker magnetism and lower crystallinity, and more definitely crystalline ferrites of magnetite (Fe_3O_4) and/or maghemite (γ-Fe_2O_3) are dispersed in the further treated samples of $n \geq 2$, as we suggested that in the preceding section. Essentially the same observations by WAXD were made for any of the other test series, 3%

ι-0.10-*n*, 5% ι-0.50-*n*, and 5% κ-0.10-*n* (*n* = 1–3). As discussed later, the feroxyhite first produced would serve as a precursor yielding the more familiar ferrites in the repeated cycle of the *in situ* synthesis process.

<<**Figure 6**>>

<<**Table 2**>>

Figure 7 shows TEM photographs of iron oxides extracted from two composites, 5% ι-0.10-1 and 5% ι-0.10-3. Photo data **a** and **b** were obtained for the former sample of *n* = 1, and photo **c** refers to the latter one of *n* = 3. As demonstrated by photo **a**, it was confirmed that iron oxide nanoparticles of ca. 15 nm in diameter were dotted in the inside of 5% ι-0.10-1. Some agglomerate composed of needle-like particles of ca. 5 nm in width and 30–60 nm in length was also observed in places on the grid specimen, as illustrated in photo **b**. This kind of morphology, i.e., a crystalline growth habit in an acicular shape, might be characteristic of the magnetic iron compound feroxyhite, as has been pointed out in an earlier study[3] on cellulose/iron oxide compositions.

<<**Figure 7 (a), (b), & (c)**>>

On the other hand, as can be seen from photo **c** in Figure 7, the composite sample 5% ι-0.10-3 accommodated more iron oxide particles in a clear-cut granulated form of ϕ = 15–40 nm. An assemblage of the granular particles, observed at a level of >100 nm, can be taken as being formed in the process of preparation of the grid specimen for TEM. The diameter size of 15–40 nm for the dispersed magnetic particles is in consistence with the condition delivering a composite material of SPM character. From major diffraction peaks (2θ = 30.1º, 35.5º, and 57.1º) appearing in the WAXD curve of 5% ι-0.10-3 (Fig. 6c), a crystallite size *L* of the produced ferrites was approximated, using a conventional Scherrer equation:

$$L = 0.9\lambda/B\cos\theta \qquad (2)$$

where λ is a wavelength (0.1542 nm) of CuKα radiation and *B* is a half-height width of the diffraction peak considered. An assessment of *L* = 10–15 nm was made, which never

conflicts with the TEM and magnetometric observations described above.

From the results of the analysis of morphological features and magnetic property for a series of composite products, it can be said that, as originally expected, the hydrogels of the anionic sulfate-containing polysaccharide, carrageenan, filled the role of a good matrix providing cavity sites suitable for the *in situ* synthesis of iron oxide nanoparticles and accommodating the magnetic assemblage of SPM character to a considerable amount.

Further Insight into Evolution of Magnetic Nanoparticles

SQUID magnetometry was also conducted for κ-carrageenan/iron oxide composites (5% κ-0.10(cop)-*n* (*n* = 1–3)) prepared by the coprecipitation method with a 1:2 mixture of ferrous/ferric ions. The characterization included magnetization measurements of *M* vs *T* as well as of *M* vs *H*. The major analytical results are summarized in Table 3, together with corresponding data for the comparable samples 5% κ-0.10-*n* obtained by the standardized *in situ* method via $Fe(OH)_2$ production with only Fe^{2+}. In the coprecipitation process under the alkaline condition adopted, Fe_30_4 is expected to mainly produce according to the following reaction:

$$Fe^{2+} + 2Fe^{3+} + 8OH^- \rightarrow Fe_3O_4 + 4H_2O \qquad (3)$$

However, the magnetite precipitate may be further oxidized into γ-$Fe_2O_3/Fe(OH)_3$ to some extent depending on the operative conditions of oxygen, temperature, and aging time.[13,15,20] WAXD measurements supported the particle formation of Fe_30_4 (and possibly of maghemite γ-Fe_2O_3) in the composites 5% κ-0.10(cop)-*n*, irrespective the cycle number *n*.

<<**Table 3**>>

In the *M* vs *H* measurements for 5% κ-0.10(cop)-*n* at 298 and 100 K, any sample of *n* = 1–3 gave a non-hysteretic loop of naught coecivity or remanence; thus the composites were all superparamagnetic even at 100 K. As listed in Table 3, values of the saturation magnetization at 298 K were estimated as M_s = 2.9 (*n* = 1), 5.6 (*n* = 2), and 9.0 (*n* = 3) in emu

(g sample)$^{-1}$. Interestingly, these were generally lower than the respective corresponding M_s values obtained for 5% κ-0.10-n, even though each pair comparable between the two composite series showed a similar degree of Fe uptake. The difference in M_s was particularly noticeable when the two series were treated in the multicycles of n = 2 and 3. From these observations, it can be inferred that the ferrite particles embedded in the matrix of 5% κ-0.10(cop)-n are of definitely smaller sizes, compared with those in the other series of 5% κ-0.10-n. This is made clearer by M vs T measurements in the zero-field-cooled (ZFC) and field-cooled (FC) modes, as shown below.

Figure 8 illustrates ZFC and FC curves obtained for two samples, 5% κ-0.10-2 (Fig. 8a) and 5% κ-0.10(cop)-2 (Fig. 8b), in an applied field of 0.01 T. For both samples, we can see a convergence of the ZFC and FC plots at higher temperatures (≥200 K for 5% κ-0.10-2 and ≥100 K for 5% κ-0.10(cop)-2) and a divergence of the two plots at lower temperatures. This kind of behavior is typical of SPM materials. In this case, the FC curve continues to increase with decreasing temperature, while the ZFC curve assumes a peak maximum at T_{max} and decreases below T_{max}. T_{max} is related to a so-called blocking temperature T_B by the following equation:[22,23]

$$T_{max} = \beta T_B \qquad (4)$$

where β is a parameter associated with size distribution of the magnetic particles concerned, typically situated in a range of 1.5–2.0. At temperatures lower than T_B, the magnetic moment of the particles is frozen along their respective anisotropy axes, so that an FM character manifests itself instead of the high-temperature SPM.[21]

<<**Figure 8 (a) & (b)**>>

In Figure 8b, the ZFC data for 5% κ-0.10(cop)-2 makes a maximum at T_{max} = 60 K, which leads to T_B = 30–40 K. Therefore, the observation of SPM in the M vs H measurement at 100 K for the same sample is quite reasonable. Contrastively, in Figure 8a, the sample encoded as 5% κ-0.10-2 imparts a broader ZFC peak with the maximum at a

higher temperature of T_{max} = 160 K. The broadening of the peak is interpreted as due to a wider distribution of particle size. From T_{max} = 160 K, we obtain T_B = 80–107 K; hence, a hysteretic FM behavior in M vs H observed at 100 K may also be reasonable (see Table 3).

In comparison between three samples (n = 1–3) of the coprecipitation series, while the magnetization at each temperature became greater with an increase in the cycle number n, the three sets of ZFC and FC data were almost identical in shape with each other, irrespective of the number n. With regard to the other series of 5% κ-0.10-n, it was observed that the ZFC peak became broader and T_{max} and T_B increased, as the *in situ* synthesis process was repeated. For the sample of n = 1, T_B = 65–87 K was estimated; nevertheless, the M vs H data at 100 K provided a hysteresis loop with nonzero values of remanent magnetization and coercive force. The presence of magnetic particles of comparatively larger sizes (e.g. ≥35 nm) should be responsible for the FM behavior at 100 K, which reflects the distribution of particle dimension still wider relative to that in the coprecipitation series.

As tabulated in Table 3, the specific saturation magnetization, M_s(Fe), for the samples of 5% κ-0.10(cop)-n was evaluated as ca. 42-45 emu (g Fe)$^{-1}$. Obviously, these values are much smaller than those of bulk ferrites, M_s(Fe) = 110–131 (for Fe_3O_4) and 100–109 (for γ-Fe_2O_3) in emu (g Fe)$^{-1}$ which are converted from M_s = 80–95 (for Fe_3O_4)[24–26] and 70–76 (for γ-Fe_2O_3)[25,27] in emu per gram of the respective iron oxides. The serious reduction in the specific magnetization may be attributed principally to the quantum-size effect in ultrafine nanoparticles (ϕ < 10 nm) that invites lack of magnetic saturation.[24,26,27] In the M vs H measurements for the 5% κ-0.10(cop)-n series, strictly, the magnetization never completely saturated at 5 T but tended to still rise with additional application of magnetic field.

In view of the comparative investigations stated above, it is possible to conclude the following: The stoichiometric coprecipitation method provides carrageenan composites containing very minute magnetic nanoparticles (e.g. 5–15 nm) of narrower size distribution, whereas, in the method via producing $Fe(OH)_2$ from only a ferrous salt, somewhat larger

magnetic nanoparticles (15–40 nm) of wider size distribution are embedded in the carrageenan composites. On equal terms in iron uptake, the former series of composites show the SPM to FM transition at a lower blocking temperature (<50 K), and the latter can display quite a high value of M_s with retaining SPM character at temperatures of >150 K. Here, it should be noted that the comparative characterizations were made between the two composite series prepared by treatment in almost the same alkaline condition at 65–70 ºC, where the carrageenan matrices remained in a clear gel form without collapsing. Therefore, the observed difference in nanoparticle dimensions may be ascribed simply to the difference in kinetics of whether the oxidization of irons (ions) into magnetic iron oxides went through an immediate pathway (referring to the coprecipitation method) or a step-by-step one (referring to the method via $Fe(OH)_2$ production).

Regarding the case where the carrageenan matrix is treated in multicycles of the standardized synthesis process, we can explicate the mechanism of growth of iron oxide nanoparticles therein, in terms of the following reaction scheme: In the first cycle (n = 1), by alkali (NaOH) treatment of ferrous ion-intercalated carrageenan ($Car\text{-}SO_3^-\text{---}Fe^{2+}\text{---}SO_3^-\text{-}Car$), $Fe(OH)_2$ precipitates inside of the polymer network (Eq. (5)). In the subsequent step of oxidation with H_2O_2, the ferrous hydroxide is transformed into δ-FeOOH, according to Equation (6).

$$Car\text{-}SO_3^-\text{---}Fe^{2+}\text{---}SO_3^-\text{-}Car + 2NaOH \rightarrow 2Car\text{-}SO_3^-\,Na^+ + Fe(OH)_2 \qquad (5)$$

$$Fe(OH)_2 + (1/2)\,H_2O_2 \rightarrow \delta\text{-}FeOOH + H_2O \qquad (6)$$

In the next cycle (n = 2), besides repetition of the above chemical reactions, freshly supplied Fe^{2+} would actively adsorb onto the feroxyhite seed to form an intermediate to Fe_3O_4 in alkaline surroundings, as indicated by Equation (7); then, the intermediate, $(\delta\text{-}FeOOH)_2FeOH^+$, may be smoothly oxidized into Fe_3O_4 (Eq. (8)).

$$2(\delta\text{-}FeOOH) + Fe^{2+} + H_2O \rightarrow (\delta\text{-}FeOOH)_2FeOH^+ + H^+ \qquad (7)$$

$$(\delta\text{-}FeOOH)_2FeOH^+ \rightarrow Fe_3O_4 + H_2O + H^+ \qquad (8)$$

This route has also been adopted by Sourty et al.,[3] but it is originally based on a mechanism of dissolution and recrystallization of γ-FeOOH (lepidocrocite) into magnetite, reported by Tamura et al..[28] A similar transformation from δ-FeOOH as precursor into MnZn ferrite has been studied by Hao et al.[29]

In the repeated cycles ($n \geq 2$), a certain quantity of Fe^{2+} ions should be oxidized into Fe^{3+} by trace amounts of oxygen that inevitably remains in the aqueous solvent after the first oxidation step. Therefore, formation of Fe_3O_4 nanoparticles in smaller sizes through the coprecipitation process according to Equation (3) may also be admitted as a concurrent route in the present *in situ* method.

Concerning the oxidation of Fe_3O_4 to its counterpart γ-Fe_2O_3, i.e., $Fe_3O_4 + (1/4)\ O_2 \rightarrow (3/2)\ \gamma$-$Fe_2O_3$, the present oxidizing condition at <70 ºC seems to be insufficient, at least in a single cycle, to the successful conversion which has been exemplified with more rigorous hydrothermal conditions.[13,25,27] However, when the magnetite-containing composite is further treated in the multicycles of $n \geq 3$, the conversion due to an aging effect[15,25] may partly occur with the passage of time.

CONCLUSION

Carrageenan-based magnetic composites were successfully prepared by the repeatable *in situ* synthesis of iron oxides in a ferrous ion-intercalated gel network of the polysaccharide, and the magnetic property and morphology of the composite products were characterized well by SQUID magnetometry, X-ray diffractometry, and electron microscopy. The evolution mechanism in oxidation state and dimensional distribution of the cyclically loaded iron oxide particles was also deliberated, through comparison with another composite series obtained by the coprecipitation method with a 1:2 mixture of ferrous/ferric ions.

All the composites prepared via only one cycle of the standardized *in situ* process showed a superparamagnetic (SPM) property at 298 K, and the respective values of saturation

magnetization (M_s) were situated in a range of 2–9 emu (g sample)$^{-1}$ with positive dependence on the ferrous salt concentration used for gel immersion. The dependence was steeper in the employment of κ-carrageenan rather than ι-carrageenan as the gel matrix. The ferrous ion-intercalated network of ι-carrageenan may be a little tighter than that of the κ type. In support of this, the ι-carrageenan composites were generally superior to the κ-carrageenan ones in the SPM retention at ≤200 K. By operation of 3–4 cycles of the standard synthesis route, both κ and ι types of carrageenan composites imparting $M_s \geq$ ~25 emu (g sample)$^{-1}$ were easily realized while the property of room temperature SPM was maintained.

The iron oxide particles loaded in the first cycle were predominantly feroxyhite (δ-FeOOH), whereas the particles present in the composites treated in the multicycles were assumed to be mainly magnetite (Fe_3O_4). Presumably, the majority of the magnetite particles were derived from the feroxyhite seeds formed in advance, and also smaller magnetite particles producible by coprecipitation from a secondary mixture of Fe^{2+}/Fe^{3+} were mingled with the acquired majority. Further oxidation of Fe_3O_4 into maghemite (γ-Fe_2O_3) might have been restricted to a small contribution of the aging effect possible in the course of preparation and storage of the composite samples.

As a morphological feature common to the composite products, it was observed that the pertinent iron oxides were produced in a particle size less than several tens of nanometers (ϕ = 15–40 nm) and dispersed in the inside as well as on the surface area of fibrillar entities constituting the gel matrix of carrageenan. The observed dimensional scale was in consistence with the SPM property that came into possession of the composites. The particle size distribution was regarded as somewhat wider relative to that (ϕ = 5–15 nm) attainable in the comparable composite series using the thoroughgoing coprecipitation. However, the latter series showed considerably lower values of magnetization against the applied magnetic field of practical magnitudes.

The carrageenan/iron oxide nanocomposites investigated in the present paper were,

virtually, all magnetically isotropic. In our subsequent study, the result obtained in this work will serve as a cornerstone in fabricating polysaccharide-based smart materials that can show an anisotropic magnetization response favorable for a diversity of dynamic functionalities.

Acknowledgments. The authors wish to acknowledge Dr. A. Otsuka of Research Center for Low Temperature and Materials Sciences, Kyoto University, for his technical assistance in the SQUID magnetometry measurements. This work was partially financed by a Grant-in-Aid for Scientific Research (A) (no. 23248026 to Y. N.) from the Japan Society for the Promotion of Science.

REFERENCES

1. Marchessault, R. H., Ricard, S. & Rioux, P. *In situ* synthesis of ferrites in lignocellulosics. *Carbohydr. Res.* **224**, 133–139 (1992).

2. Raymond, L., Revol, J. -F., Ryan, D. H. & Marchessault, R. H. *In situ* synthesis of ferrites in cellulosics. *Chem. Mater.* **6**, 249–255 (1994).

3. Sourty, E., Ryan, D. H. & Marchessault, R. H. Characterization of magnetic membranes based on bacterial and man-made cellulose. *Cellulose* **5**, 5–17 (1998).

4. Suber, L., Foglia, S., Ingo, G. M. & Boukos, N. Synthesis, and structural and morphological characterization of iron oxide-ion-exchange resin and -cellulose nanocomposites. *Appl. Organometal. Chem.* **15**, 414–420 (2001).

5. Chatterjee, J., Haik, Y. & Chen, C. J. Biodegradable magnetic gel: synthesis and characterization. *Colloid Polym. Sci.* **281**, 892–896 (2003).

6. Nishio, Y. Material functionalization of cellulose and related polysaccharides via diverse microcompositions. *Adv. Polym. Sci.* **205**, 97–151 (2006).

7. Matsumoto, Y., Teramoto, Y., & Nishio, Y. Preparation of thermoplastic magnetic wood via etherification and *in-situ* synthesis of iron oxide. *J. Wood Chem. Tech.* **30**, 373–381

(2010).

8. Liu, S., Zhou, J. & Zhang, L. In situ synthesis of plate-like Fe_2O_3 nanoparticles in porous cellulose films with obvious magnetic anisotropy. *Cellulose* **18**, 663–673 (2011).

9. Kroll, E., Winnik, F. M. & Ziolo, R. F. In situ preparation of nanocrystalline γ-Fe_2O_3 in Iron(II) cross-linked alginate gels. *Chem. Mater.* **8**, 1594–1596 (1996).

10. Veiga, V., Ryan, D. H., Sourty, E., Llanes, F. & Marchessault, R. H. Formation and characterization of superparamagnetic cross-linked high amylose starch. *Carbohydrate Polymers.* **42**, 353–357 (2000).

11. Jones, F., Cölfen, H. & Antonietti, M. Interaction of κ-carrageenan with nickel, cobalt, and iron hydroxides. *Biomacromolecules* **1**, 556–563 (2000).

12. Pardoe, H., Chua-anusorn, W., St. Pierre, T. G. & Dobson, J. Structural and magnetic properties of nanoscale iron oxide particles synthesized in the presence of dextran or polyvinyl alcohol. *J. Magn. Magn. Mater.* **225**, 41–46 (2001).

13. Kim, D. K., Mikhaylova, M., Zhang, Y. & Muhammed, M. Protective coating of superparamagnetic iron oxide nanoparticles. *Chem. Mater.* **15**, 1617–1627 (2003).

14. Nishio, Y., Yamada, A., Ezaki, K., Miyashita, Y., Furukawa, H. & Horie, K. Preparation and magnetometric characterization of iron oxide-containing alginate/poly(vinyl alcohol) networks. *Polymer* **45**, 7129–7136 (2004).

15. Daniel-da-Silva, A. L., Trindade, T., Goodfellow, B. J., Costa, B. F. O., Correia, R. N. & Gil, A. M. In situ synthesis of magnetite nanoparticles in carrageenan gels. *Biomacromolecules* **8**, 2350–2357 (2007).

16. Ziolo, R. F., Giannelis, E. P., Weinstein, B. A., O'Horo, M. P., Ganguly, B. N., Mehrotra, V., Russell, M. W. & Huffman, D. R. Matrix-mediated synthesis of nanocrystalline γ-Fe_2O_3: a new optically transparent magnetic material. *Science* **257**, 219–223 (1992).

17. Van de Velde, F. & De Ruiter, G. A. Carrageenan. In: *Polysaccharides II. polysaccharides from eukaryotes, Biopolymers, Vol. 6* (eds. Vandamme, E. J., De Baets, S. & Steinbüchel, A.)

(Wiley-VCH: Weinheim 2002), pp. 245–273.

18. Clark, A. H. & Ross-Murphy, S. B. Structural and mechanical properties of biopolymer gels. *Adv. Polym. Sci.* **83**, 57–192 (1987).

19. Morris, E. R., Rees, D. A. & Robinson, G. Cation-specific aggregation of carrageenan helices: domain model of polymer gel structure. *J. Mol. Biol.* **138**, 349–362 (1980).

20. Tartaj, P., Morales, M. P., González-Carreño, T., Veintemillas-Vedaguer, S. & Serna, C. J. Advances in magnetic nanoparticles for biotechnology applications. *J. Magn. Magn. Mater.* **290–291**, 28–34 (2005).

21. *Introduction to Magnetic Materials, Second Edition.* (eds. Cullity, B. D. & Graham, C. D.) (John Wiley & Sons, Inc.: Hoboken, NJ 2008).

22. Gittleman, J. I., Abeles, B. & Bozoeski, S. Superparamagnetism and relaxation effects in granular Ni-SiO_2 and Ni-Al_2O_3 films. *Phys. Rev. B* **9**, 3891–3897 (1974).

23. Tang, B. Z., Geng, Y., Lam, J. W. Y., Li, B., Jing, X., Wang, X., Wang, F., Pakhomov, A. B. & Zhang, X. X. Processible nanostructured materials with electrical conductivity and magnetic susceptibility: Preparation and properties of maghemite/polyaniline nanocomposite films. *Chem. Mater.* **11**, 1581–1589 (1999).

24. De Cuyper, M., Müller, P., Lueken, H. & Hodenius, M. Synthesis of magnetic Fe_3O_4 particles covered with a modifiable phospholipid coat. *J. Phys.: Condens. Matter* **15**, S1425–S1436 (2003).

25. Zhu, H., Yang, D., Zhu, L., Yang, H., Jin, D. & Yao, K. A facile two-step hydrothermal route for the synthesis of γ-Fe_2O_3 nanocrystals and their magnetic properties. *J. Mater. Sci.* **42**, 9205–9209 (2007).

26. Rajan, G. S., Stromeyer, S. L., Mauritz, K. A., Miao, G., Mani, P., Shamsuzzoha, M., Nikles, D. E. & Gupta, A. Superparamagnetic nanocomposites based on poly(styrene-*b*-ethylene/butylene-*b*-styrene)/cobalt ferrite compositions. *J. Magn. Magn. Mater.* **299**, 211–218 (2006).

27. Sohn, B. H., Cohen, R. E. & Papaefthymiou, G. C. Magnetic properties of iron oxide nanoclusters within microdomains of block copolymers. *J. Magn. Magn. Mater.* **182**, 216–224 (1998).

28. Tamura, Y., Ito K. & Katsura, T. Transformation of γ-FeO(OH) to Fe_3O_4 by adsorption of iron(II) ion on γ-FeO(OH). *J. Chem. Soc. Dalton Trans.* **2**, 189–194 (1983).

29. Hao, S., Wang, X., Wei, Y., Wang, Y. & Liu, C. Preparation and properties of nanosize MnZn ferrite from δ-FeOOH. *Rare Metals* **25**, 466–470 (2006).

Captions for Figures

Figure 1. Idealized repeating disaccharide structure of ι-carrageenan (R = SO_3^-) and κ-carrageenan (R = H), composed of 1,3-linked β-D-galactopyranose and 1,4-linked 3,6-anhydro-α-D-galactopyranose.

Figure 2. Magnetization vs applied magnetic field plots. (a) Data obtained at 298 K for 5% ι-0.10-*n*: △, *n* = 1; □, *n* = 2; ○, *n* = 3. (b) Data for 5% ι-0.10-3 measured at different temperatures: ●, 100 K; ○, 298 K. Insets provide the data on an enlarged scale.

Figure 3. Plots of saturation magnetization data for various series of iron oxide-incorporated carrageenan composites: (a) M_s vs Fe^{2+} concentration in gel immersion; (b) M_s vs number of reaction cycle; (c) M_s(Fe) vs number of reaction cycle. Plots in (a) are constructed for *x*% ι-*y*-1 (*x* = 3, 5, 8) and *x*% κ-*y*-1 (*x* = 3, 5), and data in both (b) and (c) are shown for *x*% ι-0.10-*n* (*x* = 3, 5) and *x*% κ-0.10-*n* (*x* = 3, 5). Starting polymer concentration (*x* %): circle, *x* = 3; square, *x* = 5; triangle, *x* = 8. Open and solid symbols refer to the ι-carrageenan and κ-carrageenan series, respectively.

Figure 4. FT-IR spectra of ι-carrageenan in a cycle of the *in situ* synthesis of iron oxides, measured at stages: (i) pristine state (after purification): (ii) after intercalation of ferrous ions; (iii) after alkali treatment; (iv) after oxidation.

Figure 5. FE-SEM photographs of fracture surfaces for ι- and κ-carrageenan composites containing iron oxides (right side: **c**, **e**, and **g**), compared with data for their respective reference samples of naught Fe content (left side: **a**, **b**, **d**, and **f**). A sample 5% ι-0.10(Ca)-1

(**b**) was prepared with $CaCl_2$ instead of $FeCl_2$ at the stage of gel immersion in the scheme of iron oxide synthesis. The other blank samples (**a**, **d**, and **f**) were obtained by skipping the gel immersion into $FeCl_2$ solution, i.e., via only two steps including alkali treatment with NaOH and oxidation with H_2O_2. Scale bars denote 200 nm. Drawings inserted into photos **e** and **g** schematically show the precipitation of iron oxide nanoparticles in the inside and on the surface area of carrageenan fibrils.

Figure 6. WAXD intensity profiles for 5% ι-0.10-*n*: (a) *n* = 1; (b) *n* = 2; (c) *n* = 3. The marking of diffraction peaks indicates that they are derived from δ-FeOOH (△) or from Fe_3O_4 and/or γ-Fe_2O_3 (●).

Figure 7. TEM photographs of iron oxides extracted from 5% ι-0.10-*n* (*n* = 1 and 3): photo **a** and **b**, data for 5% ι-0.10-1; photo **c**, data for 5% ι-0.10-3.

Figure 8. Temperature dependence of magnetization in a field of 0.01 T, measured for (a) 5% κ-0.10-2 and (b) 5% κ-0.10(cop)-2. FC and ZFC curves were obtained for each sample with and without the field prior to the measurement, respectively.

In addition to the eight figures, there are three tables. See annexed sheets.

Table 1. Magnetic properties of iron oxide-containing carrageenan composites prepared under different conditions

Table 2. 2θ values of the diffraction peaks observed for 5% ι-0.10-*n* (*n* = 1–3) (see Fig. 6), and comparable JCPDS data for Fe_3O_4, γ-Fe_2O_3, and δ-FeOOH

Table 3. Comparison of magnetic properties between the two series of composites, 5% κ-0.10-*n* and 5% ι-0.10(cop)-*n* (*n* = 1–3), the former prepared by the standardized *in situ*

method via producing $Fe(OH)_2$ with only Fe^{2+} and the latter by the coprecipitation method with a 1:2 mixture of Fe^{2+}/Fe^{3+}

GRAPHICAL ABSTRACT

Nanoincorporation of iron oxides into carrageenan gels and magnetometric and morphological characterizations of the composite products

Kazuyuki Oya, Takahiro Tsuru, Yoshikuni Teramoto, and Yoshiyuki Nishio

Carrageenan-based magnetic composites were prepared via *in situ* synthesis of iron oxides in a gelatinous network of the polysaccharide. Magnetic properties and morphology were characterized by SQUID magnetometry, X-ray diffractometry, and electron miscroscopy. By operation of 3–4 cycles of the standard synthesis route, a carrageenan composite imparting a high value of saturation magnetization (~25 emu (g sample)$^{-1}$) was easily realized while the superparamagnetic property at room temperature was maintained. Insight was provided into the evolution mechanism in oxidation state and dimensional distribution of the cyclically loaded iron oxide nanoparticles.

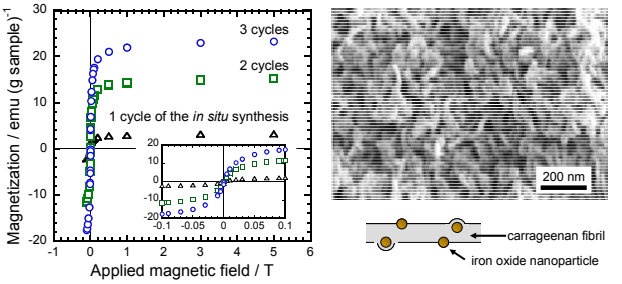

Carrageenan-based magnetic composites prepared via *in situ* synthesis of iron oxides

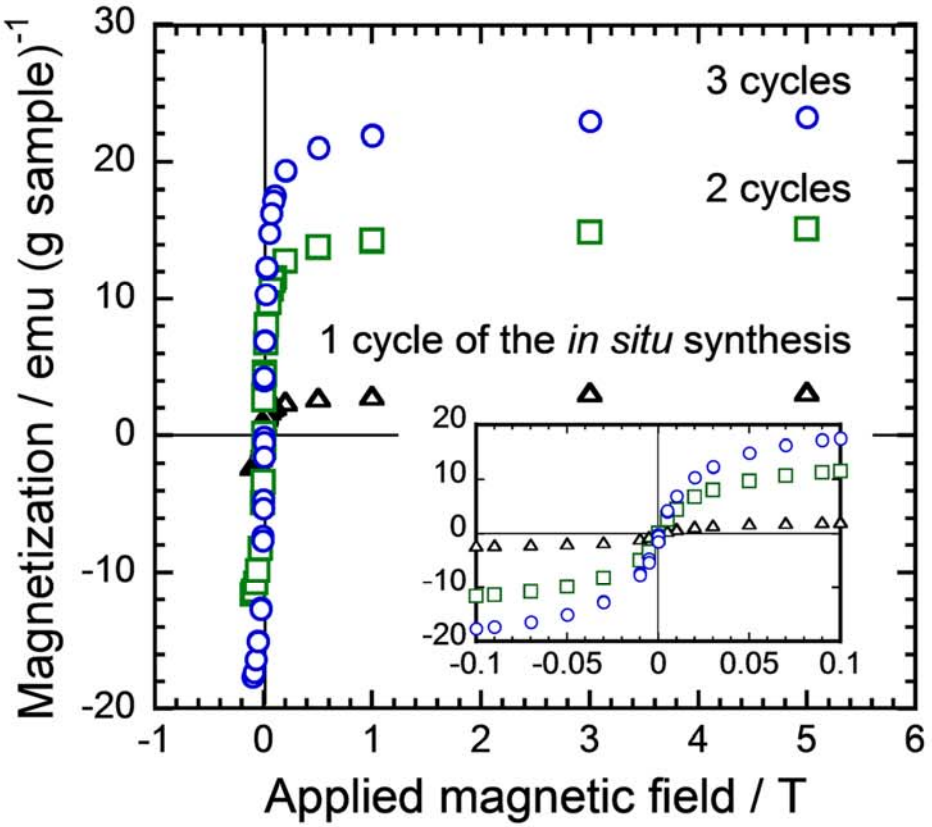

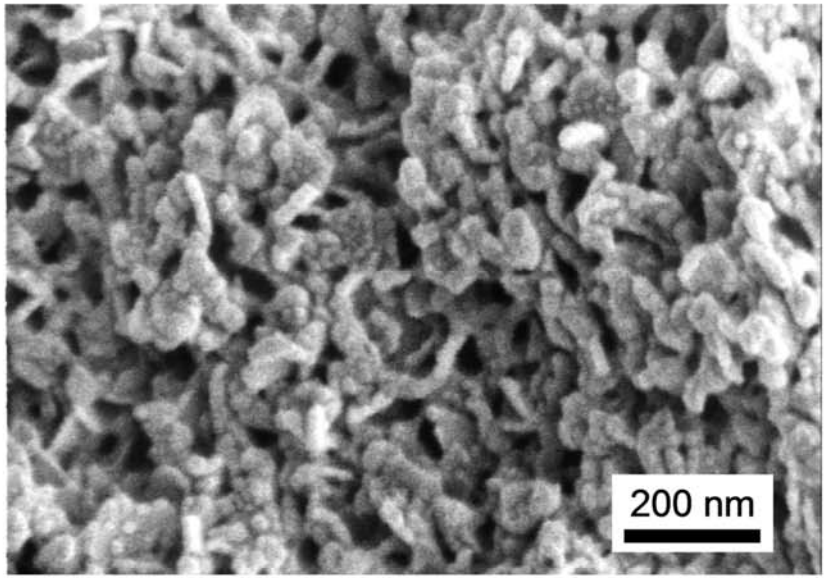

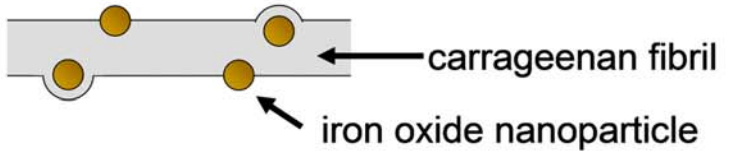

Carrageenan-based magnetic composites prepared via *in situ* synthesis of iron oxides

Table 1. Magnetic properties of iron oxide-containing carrageenan composites prepared under different conditions

	Fe content	Magnetism[a]			Saturation magnetization at 298 K	
Sample code	/wt%	100 K	200 K	298 K	M_s/emu (g sample)$^{-1}$	M_s(Fe)/emu (g Fe)$^{-1}$
5% ι-0.01-1	6.7	FM	SPM	SPM	2.3	33.5
5% ι-0.10-1	8.1	FM	SPM	SPM	2.9	36.0
5% ι-0.50-1	14.4	FM	FM	SPM	4.7	32.7
5% κ-0.01-1	5.1	FM	FM	SPM	1.5	28.6
5% κ-0.10-1	8.7	FM	FM	SPM	3.2	37.1
5% κ-0.50-1	22.3	FM	FM	SPM	8.6	38.4
3% ι-0.10-1	8.2	FM	FM	SPM	2.6	31.4
3% κ-0.10-1	10.4	FM	FM	SPM	3.9	37.3
8% ι-0.10-1	8.2	FM	SPM	SPM	3.0	36.4
5% ι-0.10-2	16.3	FM	SPM	SPM	14.3	87.8
5% ι-0.10-3	21.6	FM	FM	SPM	21.9	101.3
5% ι-0.10-4	25.8	FM	FM	SPM	27.1	105.0
5% ι-0.10-5	31.5	FM	FM	FM	31.4	99.6

[a] FM, ferromagnetic; SPM, superparamagnetic.

Table 2. 2θ values of the diffraction peaks observed for 5% ι-0.10-n (n = 1–3) (see Fig. 6), and comparable JCPDS data for Fe_3O_4, γ-Fe_2O_3, and δ-FeOOH

Values observed for 5% ι-0.10-n			Data of standards		
n = 1	n = 2	n = 3	Fe_3O_4[a]	γ-Fe_2O_3[b]	δ-FeOOH[c]
35.18	30.10	30.12	30.14	30.26	35.28
40.40	35.46	35.48	35.52	35.64	40.00
54.22	43.22	43.12	43.06	43.31	54.52
63.16	53.60	53.60	53.49	53.74	63.20
	57.12	57.12	56.98	57.37	
	62.78	62.76	62.53	62.93	

[a] JCPDS card 19-629; [b] JCPDS card 39-1346; [c] JCPDS card 13-87.

Table 3. Comparison of magnetic properties between the two series of composites, 5% κ-0.10-n and 5% ι-0.10(cop)-n (n = 1–3), the former prepared by the standardized *in situ* method via producing $Fe(OH)_2$ with only Fe^{2+} and the latter by the coprecipitation method with a 1:2 mixture of Fe^{2+}/Fe^{3+}

Sample code	Fe content (wt%)	Magnetism[a]		Saturation magnetization at 298 K		Temperatures referring to blocking phenomenon[b]	
		100 K	298 K	M_s /emu (g sample)$^{-1}$	M_s(Fe) /emu (g Fe)$^{-1}$	T_{max}/K	T_B/K
5% κ-0.10-1	8.7	FM	SPM	3.2	37.1	130	65–87
5% κ-0.10-2	15.4	FM	SPM	13.1	85.5	160	80–107
5% κ-0.10-3	25.9	FM	SPM	23.3	90.0	230	115–153
5% κ-0.10(cop)-1	6.3	SPM	SPM	2.9	45.1	60	30–40
5% κ-0.10(cop)-2	13.6	SPM	SPM	5.6	41.2	60	30–40
5% κ-0.10(cop)-3	20.8	SPM	SPM	9.0	43.3	70	35–47

[a] FM, ferromagnetic; SPM, superparamagnetic.

[b] T_{max}, temperature giving a ZFC peak maximum in M vs T measurements; T_B, blocking temperature approximated from $T_{max} = \beta T_B$ (β = 1.5–2.0).

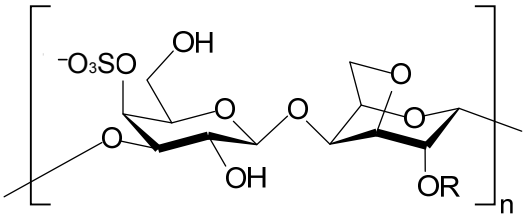

Figure 1.

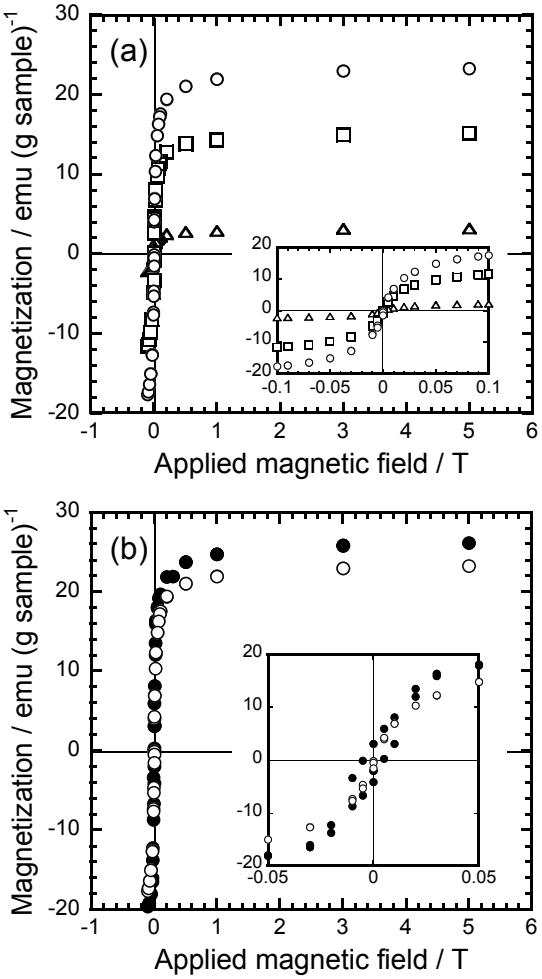
(a)
Magnetization / emu (g sample)$^{-1}$
Applied magnetic field / T
(b)
Magnetization / emu (g sample)$^{-1}$
Applied magnetic field / T

Figure 2.

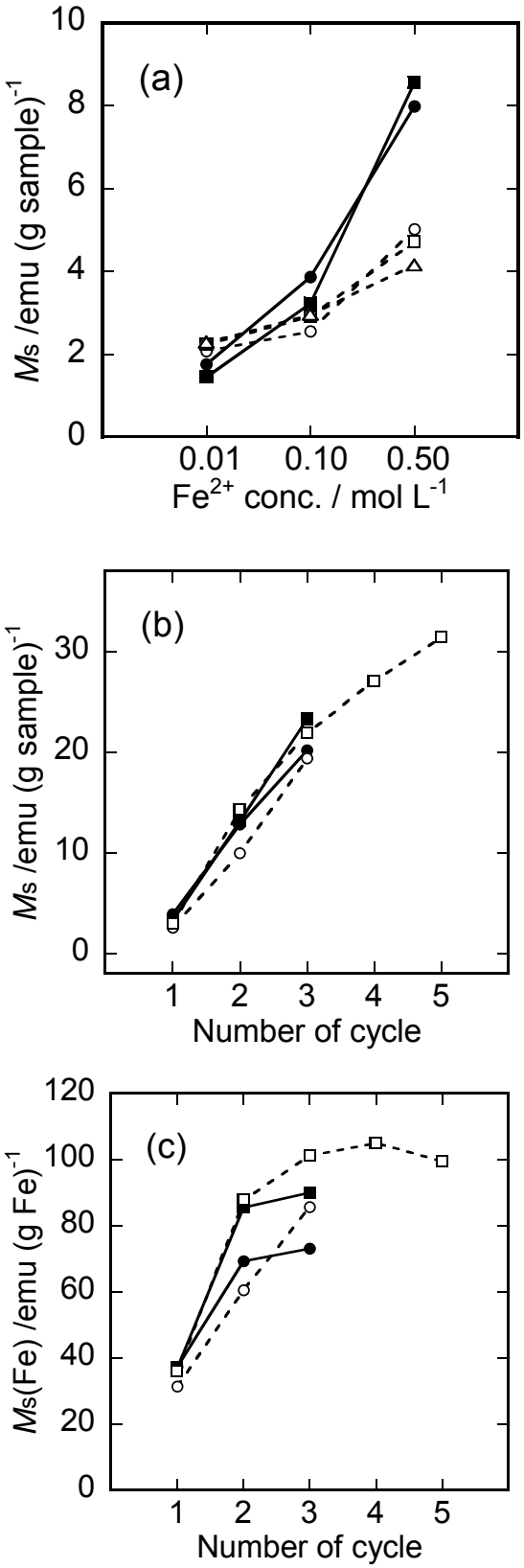
(a)
Ms /emu (g sample)-1
Fe2+ conc. / mol L-1
0.01
0.10
0.50
(b)
Ms /emu (g sample)-1
Number of cycle
(c)
Ms(Fe) /emu (g Fe)-1
Number of cycle

Figure 3.

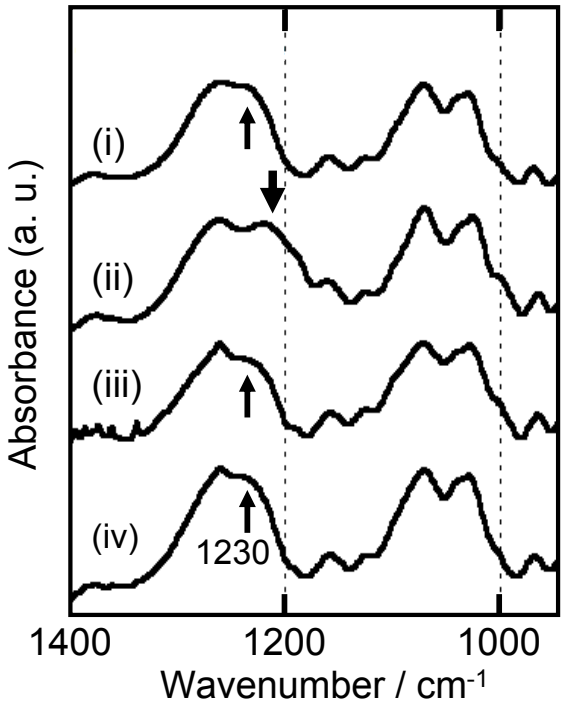

Figure 4.

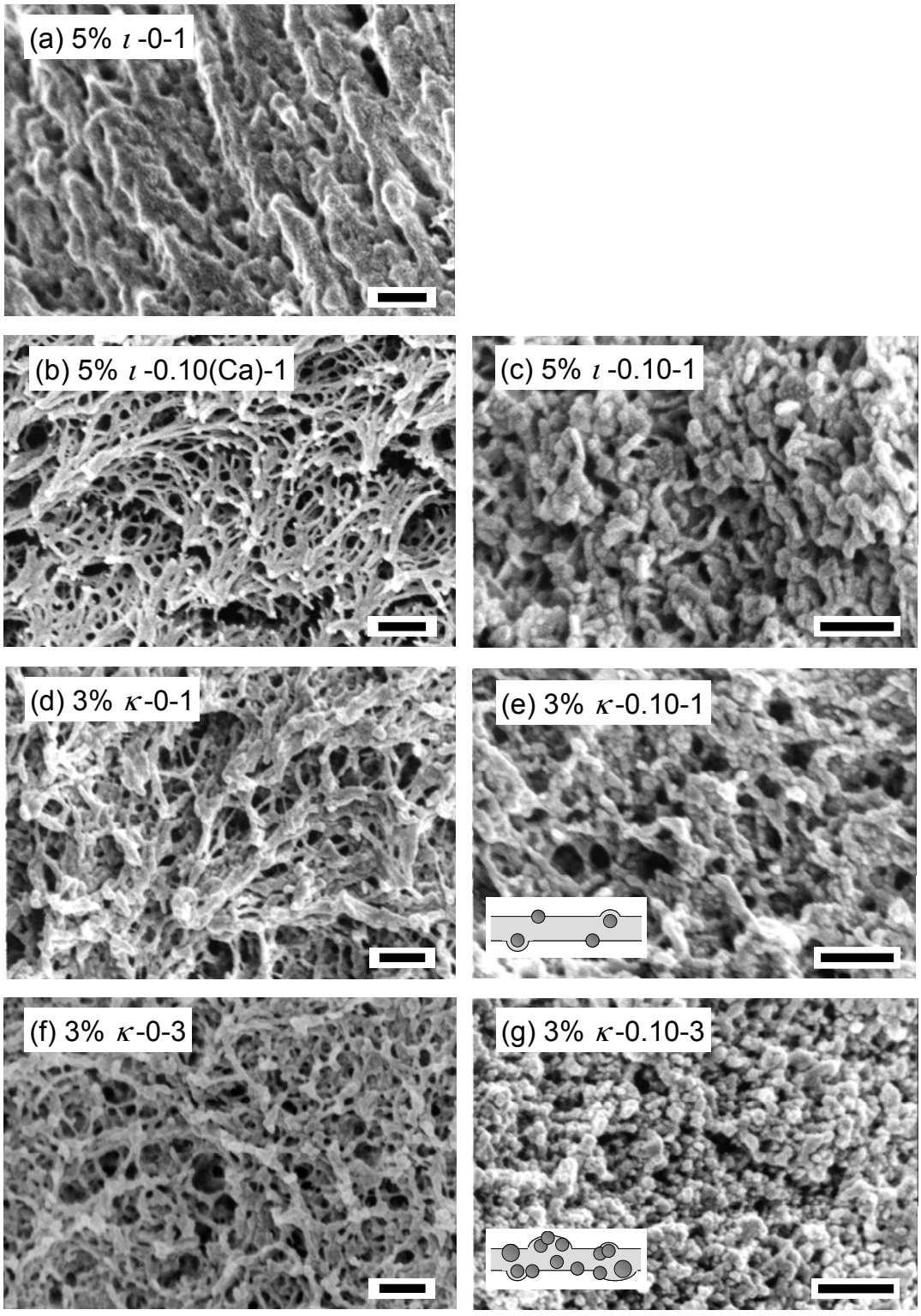

Figure 5.

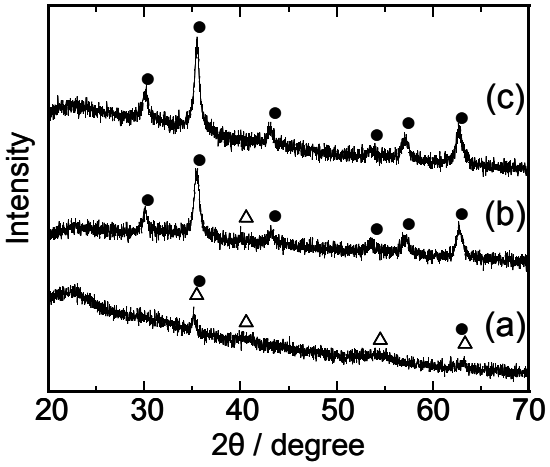

Figure 6.

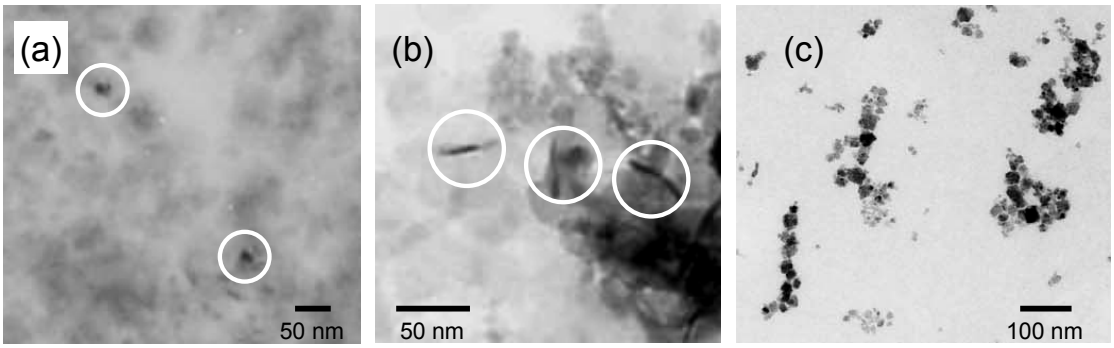

Figure 7.

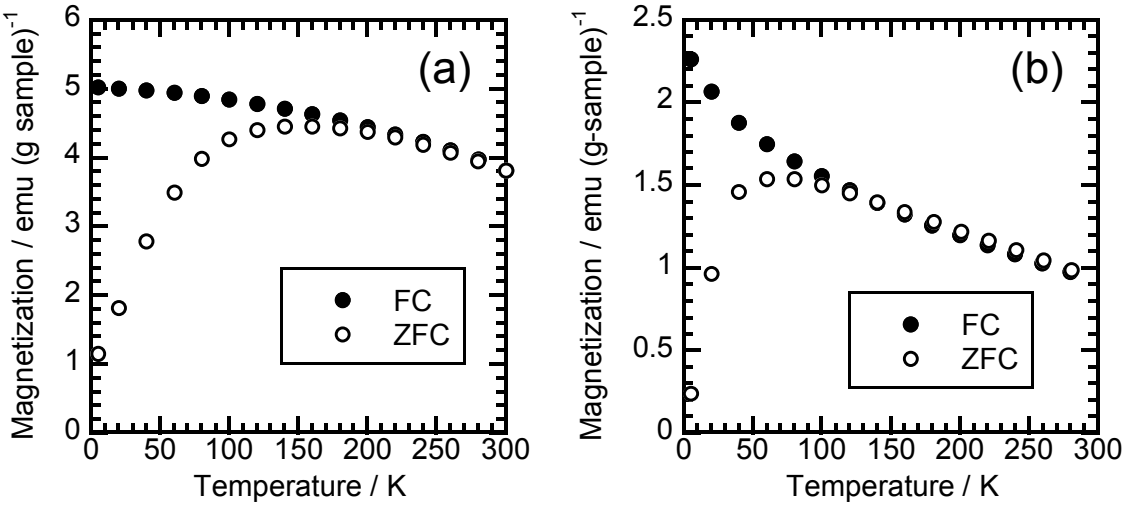
(a)
(b)
FC
ZFC
Magnetization / emu (g sample)$^{-1}$
Magnetization / emu (g-sample)$^{-1}$
Temperature / K
0
50
100
150
200
250
300
0
1
2
3
4
5
6
0
0.5
1
1.5
2
2.5

Figure 8.